



HAL
open science

The shape of the elemental system in a porous medium designed for thermochemical energy storage

Alexandre Malley-Ernewein, Sylvie Lorente

► **To cite this version:**

Alexandre Malley-Ernewein, Sylvie Lorente. The shape of the elemental system in a porous medium designed for thermochemical energy storage. *International Journal of Heat and Mass Transfer*, 2020, 158, pp.119975. 10.1016/j.ijheatmasstransfer.2020.119975 . hal-02935549

HAL Id: hal-02935549

<https://hal.insa-toulouse.fr/hal-02935549>

Submitted on 1 Jul 2022

HAL is a multi-disciplinary open access archive for the deposit and dissemination of scientific research documents, whether they are published or not. The documents may come from teaching and research institutions in France or abroad, or from public or private research centers.

L'archive ouverte pluridisciplinaire **HAL**, est destinée au dépôt et à la diffusion de documents scientifiques de niveau recherche, publiés ou non, émanant des établissements d'enseignement et de recherche français ou étrangers, des laboratoires publics ou privés.



Distributed under a Creative Commons Attribution - NonCommercial 4.0 International License

The shape of the elemental system in a porous medium designed for Thermochemical Energy Storage

Alexandre Malley-Ernewein¹, Sylvie Lorente^{1,2*}

¹LMDC, Université de Toulouse, UPS, INSA, Toulouse, France

²Villanova University, Department of Mechanical Engineering, Villanova, PA 19085, USA

Abstract

Here we document how the design of the elemental component of a designed reactor for thermochemical energy storage can be improved for better energy performance and less pumping power. The pore channels are made of cylinders with walls are covered by salt reacting with the water vapor molecules of the blown humid air. The design of such open systems is changed to dendritic configurations while keeping the salt and fluid volumes constant. Morphing the configuration from I-shaped to Y-shaped architectures allows to increase the heat exchanges. Additional improvements are obtained when the geometric features of the dendritic configurations are chosen to follow constructal design.

Keywords: thermochemical energy storage; constructal; porous reactor

* Corresponding author: sylvie.lorente@villanova.edu

Nomenclature

Symbols

a	advancement
c	water vapor molar concentration, mol/m ³
c _p	heat capacity, J/(kg K)
d	distance between Y-shaped channel outlets, m
D	channel width, m
D _h	hydraulic diameter, m
D _v	water vapor diffusion coefficient, m ² /s
e	salt layer thickness, m
Δh	molar enthalpy of reaction, J/mol
k	thermal conductivity, W/(m K)
k _{cin}	kinetic coefficient, 1/s
L	channel length, m
\dot{m}	mass flow rate, kg/s
n	bulk molar concentration, mol/m ³
p	pressure, Pa
p _v	water vapor pressure, Pa

Re	Reynolds number
S	interface (or exchange surface) between salt and fluid, m ²
Sv	Svelteness number
T	temperature, K
t	time, s
u	velocity vector, m/s

Greek symbols

α	bifurcation angle
β	energy performance indicator
γ	reaction stoichiometric coefficient
λ	Lagrange multipliers coefficient
μ	dynamic viscosity, Pa s
ν	kinematic viscosity, m ² /s
ρ	density, kg/m ³
Φ	aggregate function

Subscripts

eq	equilibrium
----	-------------

f	fluid
I_{\max}	maximal value for the I-shaped configuration
in	inlet
init	initial
s	salt

1. Introduction

Tree-shaped networks are an icon of constructal design [1–5]. Dendritic shapes are ubiquitous both in nature (river basins, blood vessels networks) and in engineering. When the objective is to connect one point to an infinite volume of points at constant fluid volume and with the smallest effort possible, it was demonstrated that the most performant architecture corresponds to a tree-shaped network [6]. The diameter ratio between parent tube and children tubes depends on the type of flow (laminar or turbulent) and on the number of children tubes [7]. This ratio can be predicted, but its value changes with the driving force. For example when the latter is a concentration difference, the best configuration in a Y-shaped assembly made of cylinders is $D_2/D_1 = 2^{-1/2}$ [8], whereas it is $D_2/D_1 = 2^{-1/3}$ [9], when a pressure difference drives the laminar movement of fluid. Yet, if the flow network is embedded within a solid which emits heat uniformly in order to extract that heat, we showed that the combination of 2 objectives – minimum pumping power and maximum heat transfer – leads to architectures that may not remain dendritic, depending on the flow characteristic parameters (Be number, Re number, level of bifurcation)[10]. An exhaustive effort was implemented recently in Refs. [11,12] for Newtonian and non-Newtonian fluids, and for constant and pulsatile flow systems. In this work,

the fluid flows through cylindrical ducts which walls are receiving a constant and uniform heat flux. The analysis accounts for the pressure losses due to friction but also for the acceleration of the fluid due to the temperature increase associated to the heat flux along each wall. Therefore the diameter ratio leading to smaller pressure losses and hence smaller pumping power depends on the strength of the heat flux.

Constructal design finds numerous applications in the domain of energy storage. The essence of heating processes and their link to the constructal law was covered recently in [13,14]. Latent energy storage designs were presented in [15–18] with the common objective of showing how the energy storage performances can be improved, while Refs. [19,20] proved the superiority of constructal designs in the design of fins for heat exchangers. Thermochemical Energy Storage which consists in storing and releasing heat by means of the chemical reaction occurring between a reactant and a gas [21,22] is receiving increasing attention in building applications mainly because heat leakages are absent from such reactions. Our previous work [23,24] demonstrated the relevance of constructal design for Thermochemical Energy Storage.

In this work, we document the merit of a dendritic network, in its elemental configuration of one pairing level, vis-à-vis a straight channel for Thermochemical Energy Storage. The networks are submitted to several driving forces: a pressure difference drives the flow of humid air, a concentration difference generates a flow of mass (represented here by water vapor), while the flow of heat comes from the non-uniform and unsteady heat released or absorbed by the salt chemical reaction on the walls of the channels.

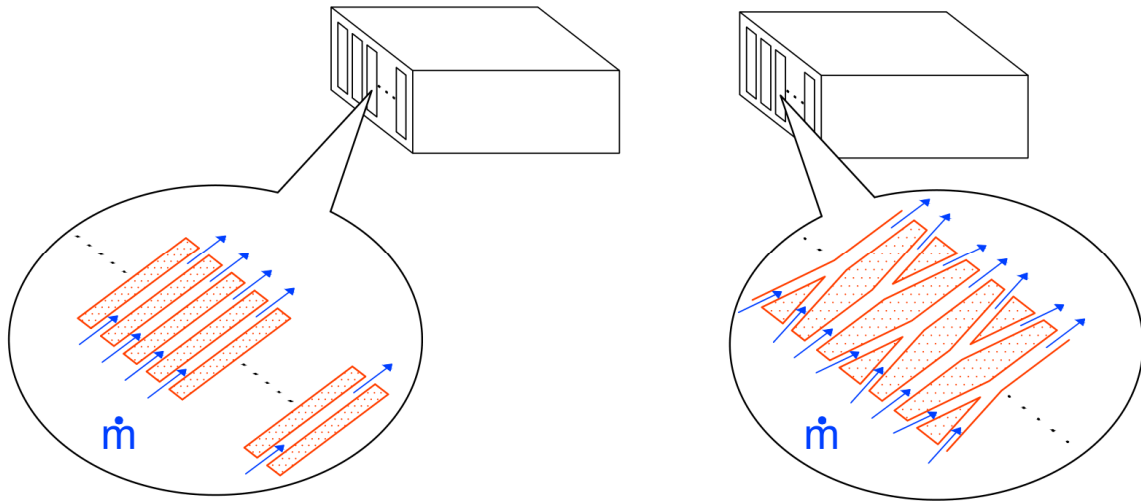


Figure 1: Two different pore configurations in a designed porous material: assemblies of straight channels or Y-shaped channels (not to scale).

The reacting module is a designed porous material which pores allow the heat transfer fluid (humid air) to cross from one side to the opposite side (Fig. 1). Because the pore walls are lined with reacting salt, the water molecules transported by the fluid flow can diffuse through the very thin salt layer (grain scale) and react with the salt. Cold humid air entering the material allows the hydration of the salt, and less humid and warmer air leaves the elemental channel through the opposite face of the porous material. In a dehydration case, hot and dry air enters the duct, the concentration difference in water molecules (under the appropriate conditions of pressure and temperature) leads to the salt dehydration and to the storage of the incoming heat.

The shape of the pores is a degree of freedom. Known are the constant mass flow rate crossing the module, the constant salt volume available and the constant fluid volume, which means that ultimately the module porosity is fixed. In this work we consider the pore as an elemental two-dimensional system. The pore could be a straight slot connecting directly one face of the module to the opposite face, or it could have a dendritic shape.

2. Configuration and model

Assume a rectilinear channel of hydraulic diameter $D_h = 2D$ which walls are covered with a thin salt layer of thickness e (Fig. 2). The length of the channel is L . The heat transfer fluid is blown through the channel while water vapor reacts with the salt thanks to a molecular diffusion process.

While the fluid volume and the salt volume are kept constant, the shape of the element is changed from an I to a Y. The fluid enters at a mass flow rate \dot{m} in the mother channel, then splits into 2 daughter tubes at a mass flow rate $\dot{m}/2$. The mother channel has a hydraulic diameter $D_{h1} = 2D_1$ and a length L_1 , while the daughter channels have a hydraulic diameter $D_{h2} = 2D_2$ and a length L_2 (Fig. 2). We have

$$DL = D_1L_1 + 2D_2L_2 \quad (1)$$

$$eL = e_1L_1 + 2e_2L_2 \quad (2)$$

where e , e_1 or e_2 are the salt thicknesses.

Such elemental configuration is aimed at being a component of a designed vascularized reactor. At first assumption the outlets (and inlets) are equidistant as in [25], and the distance between the two outlets is termed d . Hence, the Y-shaped configurations exhibit two degrees of freedom: the hydraulic diameter ratio and the length ratio (or angle of bifurcation α).

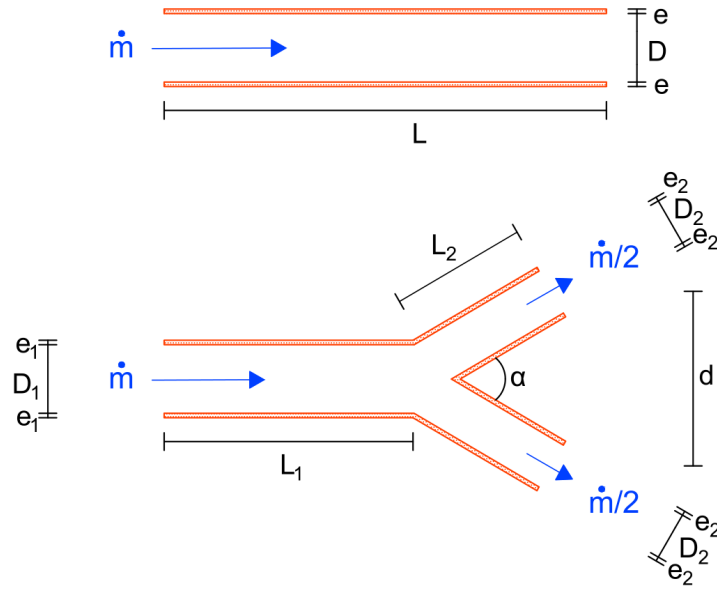


Figure 2: I-shaped and Y-shaped channels (not to scale). The total fluid volume is fixed, together with the salt volume and the mass flow rate.

Considering the fluid mechanics aspect only, the pressure drop along a slot of thickness D and length L varies, in laminar flow, as $\dot{m} L/D^3$ [26]. The straight slot represents the reference case, and its corresponding flow resistance is given by:

$$\left(\frac{\Delta p}{\dot{m}}\right)_{\text{I-shaped}} \sim \frac{L}{D^3} \quad (3)$$

The Y-shaped channel flow resistance is:

$$\frac{\Delta p}{\dot{m}} \sim \frac{L_1}{D_1^3} + \frac{L_2}{2D_2^3} \quad (4)$$

The latter is minimum for a constant fluid volume when the D_i ratio is $D_2/D_1 = 2^{-1/2}$. This result is obtained by invoking the method of the Lagrange multipliers. The aggregate function Φ is constructed from the flow resistance and the constant channels volume (assuming a unitary thickness).

$$\Phi = \frac{L_1}{D_1^3} + \frac{L_1}{2D_2^3} + \lambda(D_1L_1 + 2D_2L_2) \quad (5)$$

$D_2/D_1 = 2^{-1/2}$ is the value for which $\partial\Phi / \partial D_1 = \partial\Phi / \partial D_2 = 0$.

Such result is meaningful provided the Svelteness number is greater than 10. The Svelteness number is a non-dimensional macroscopic parameter that allows at a glance to determine if and when the local pressure losses can be neglected when compared to the friction losses [27]. $Sv \cong 10$ is the minimum value for which such assumption is acceptable. Here, we define Sv as $(L_1 + L_2)/(D_1L_1 + 2D_2L_2)^{1/2}$. In every configuration considered, $Sv > 10$.

Finally the pressure drop becomes:

$$\frac{\Delta p}{\dot{m}} \sim \frac{1}{D_1^2} (L_1 + 2^{1/2}L_2) \quad (6)$$

or

$$\frac{\Delta p}{\dot{m}} \sim \frac{(L_1 + L_2)^2}{D_1^3 Sv^2} \quad (7)$$

The problem is described thanks to mass conservation for the humid air in the channel (Eq. (8)), mass conservation for the water vapor in the channel and in the salt layer (Eqs. (9) and (10)) and momentum conservation for laminar flow in the channel (Eq. (11)). The first law of thermodynamics is written along the tube and through the salt (Eqs. (12) and (13)). Finally the reaction kinetics equation gives the reaction advancement rate for the hydration (Eq. (14)) and for the dehydration (Eq. (15)).

$$\frac{D\rho_f}{Dt} = 0 \quad (8)$$

where ρ_f is the humid air density. It is assumed that the changes in water vapor content do not impact the humid air properties [28].

$$\frac{Dc}{Dt} + \nabla(-D_{v,f}\nabla c) = 0 \quad (9)$$

where c is the water vapor concentration, and $D_{v,f}$ is the diffusion coefficient of vapor in the fluid.

$$\frac{\partial c}{\partial t} + \nabla(-D_{v,s}\nabla c) = -\gamma n_s \frac{\partial a}{\partial t} \quad (10)$$

where $D_{v,s}$ is the diffusion coefficient of vapor in the salt, γ is the reaction stoichiometric coefficient, n_s is the salt bulk molar concentration and a is the reaction advancement.

$$\frac{D\mathbf{u}}{Dt} = -\frac{1}{\rho_f}\nabla p + \nu\nabla^2\mathbf{u} \quad (11)$$

where \mathbf{u} is the velocity vector, p is the fluid pressure and ν is the kinematic viscosity.

$$\rho_f c_{p_f} \frac{DT}{Dt} + \nabla \cdot (k_f \nabla T) = 0 \quad (12)$$

where c_{p_f} is the fluid heat capacity, T is the temperature and k_f is the fluid thermal conductivity.

$$c_{p_s} \frac{\partial T}{\partial t} + \nabla \cdot (k_s \nabla T) = n_s \frac{\partial a}{\partial t} \Delta h \quad (13)$$

where c_{p_s} is the salt heat capacity, k_s is the salt thermal conductivity and Δh is the reaction heat.

$$\frac{\partial a}{\partial t} = k_{cin} \left(1 - \frac{p_{eq}}{p_v}\right) (1 - a) \quad (14)$$

$$\frac{\partial a}{\partial t} = k_{cin} \left(1 - \frac{p_{eq}}{p_v}\right) a \quad (15)$$

where k_{cin} is the reaction kinetic coefficient, p_{eq} is the equilibrium pressure, and p_v is the vapor partial pressure.

The boundary and initial conditions are the following: at the entrance of the fluid channel, the water vapor concentration, c_{in} , and the temperature, T_{in} , are fixed. An entrance length greater than $0.05 Re_{D_h} \times D$ is fixed to ensure that the flow is fully developed [29]. The inlet mass flow rate \dot{m} is constant. The outlet boundary conditions are atmospheric pressure and thermal outflow. The walls of the channels are thermally insulated without any vapor flux. A no-slip condition is imposed at the interface between fluid and salt.

The initial temperature of the system is T_{init} ($T_{init} < T_{in}$), the fluid is at rest and at atmospheric pressure, the initial vapor concentration is c_{init} corresponding to the equilibrium vapor pressure at temperature T_{init} ($c_{init} < c_{in}$). Table 1 gives the set of data. The salt characteristics are the ones of the $SrBr_2$ [28].

Table 1: Data used in the numerical simulations, adapted from [24,28].

Initial and boundary conditions		Materials thermophysical properties	
T_{init} (°C)	20	ρ_f (kg/m ³)	1.179
$T_{in,hydration}$ (°C)	25	μ (Pa.s)	$1.830 \cdot 10^{-5}$
$T_{in,dehydration}$ (°C)	80	c_{p_f} (J/(kg.K))	1011.9
$p_{v,init}$ (Pa)	137	k_f (W/(m.K))	0.026
$p_{v,in,hydration}$ (Pa)	997	$D_{v,f}$ (m ² /s)	$2.6 \cdot 10^{-5}$
$p_{v,in,dehydration}$ (Pa)	2557	$D_{v,s}$ (m ² /s)	$1.2 \cdot 10^{-13}$
c_{init} (mol/m ³)	0.056	ρ_s = $\rho_{fully\ dehydrated}$ + $a(\rho_{fully\ hydrated}$ - $\rho_{fully\ dehydrated})$ (kg/m ³)	$\rho_{fully\ dehydrated} =$ 3481 $\rho_{fully\ hydrated} =$ 2390
$c_{in,hydration}$ (mol/m ³)	0.406	c_{p_s} = $c_{p_s,fully\ dehydrated}$ + $a(c_{p_s,fully\ hydrated}$ - $c_{p_s,fully\ dehydrated})$ (J/(kg.K))	$c_{p_s,fully\ dehydrated} =$ 456 $c_{p_s,fully\ hydrated} =$ 968
$c_{in,dehydration}$ (mol/m ³)	0.893	n_s (mol/m ³)	4144.8
\dot{m}_{in} (kg/s)	$4.98 \cdot 10^{-10}$	k_s (W/(m.K))	1

The set of equations is solved by means of a FEM code [30]. Validation was made by comparing the numerical results to experimental ones in a different configuration. The details were carefully presented in a previous paper [23]. Rectangular elements of constant thickness are placed along the salt thickness, the elements shape in the fluid is rectangular except in the vicinity of the

bifurcation (see Fig. 3). The strategy chosen was based on the verification of both mass and energy conservation. Mass conservation was found much less sensitive to the mesh fineness than energy conservation. The mesh was refined regularly from one test to the other one, until the relative difference in the result of energy conservation was below 1%. Based on this assessment, 10 elements were located on the transversal direction of the salt. From the fluid/salt interface to the mid distance $D/2$, a sensitivity analysis proved that 15 elements are sufficient away from the bifurcation. They are very thin at the fluid/salt interface and increase in size when moving toward the center of the channel. The maximum thickness ratio is 5. The elements in the fluid flow direction are 4 000, equidistantly positioned. In the case of Y-shaped channels, the elements size both in the fluid and in the salt are even more refined. Finally, the number of elements is 116 000 for the I-shaped configuration, and from 100 000 to 250 000 depending on the value of the bifurcation angle in the Y-shaped designs. It takes about 2000 hours to obtain full salt hydration. For example full hydration happened after 1850 hours of exposure to humid air in the case of the Y-shaped channel with a bifurcation angle of 50° . A carefully study was implemented, reducing the time step until no change in results was noticed from one simulation to the other one. A time step of 1 hour appeared to fulfill this requirement.

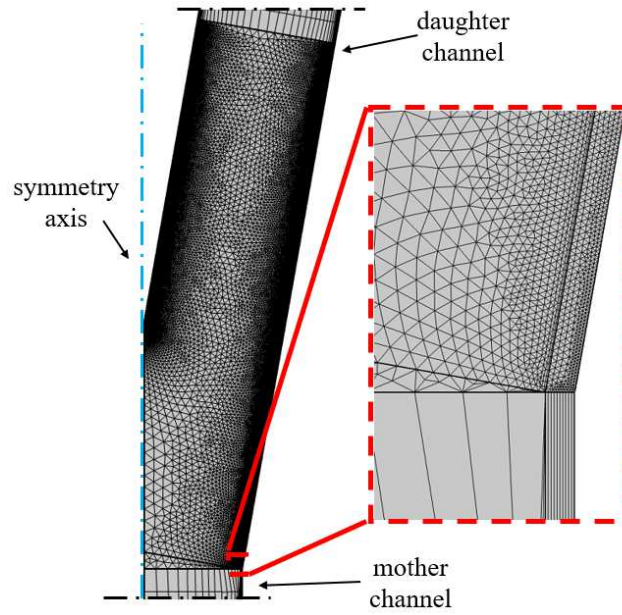


Figure 3: Example of mesh for a Y-shaped configuration. Global view of the bifurcation (left) and detail of the mesh at the junction between the mother duct and bifurcation.

3. Y or I-shaped architecture

First, the thickness of the module was allowed to decrease when moving from the straight pore to the dendritic one (see Fig. 4). We also chose $D_1 = D$ while the fluid and salt volumes remained fixed. Under such assumptions, the friction losses corresponding to the Y-shaped configuration become

$$\frac{\Delta p}{\dot{m}} \sim \frac{1}{D^3} (L_1 + 2^{1/2}L_2) \quad (16)$$

And because the amount of fluid is constant,

$$\left(\frac{\Delta p}{\dot{m}}\right)_{Y\text{-shaped}} = \left(\frac{\Delta p}{\dot{m}}\right)_{I\text{-shaped}} \quad (17)$$

In other words, we work first at identical fluid mechanics performance and look for thermal improvements. The aim of the Y-shaped design is to increase the size of the interface between the heat transfer fluid and the reacting salt. The salt thickness is assumed to remain the same along the mother and the 2 daughter tubes. Its value is obtained from the definition of the constant salt volume (Eq. (2)). Table 2 and Fig. 4 summarize the configurations obtained. The last column is the relative difference between the heat transfer exchange surface (fluid/salt interface) in the Y-shaped arrangement and the I-shaped configuration.

Table 2: Y-shaped configurations for constant salt and fluid volumes, and constant inlet width D.

α (degree)	L_2 / L_1	Relative increase in heat transfer exchange surface compared to the I-shaped design (%)
120	0.06	3.3
50	0.14	6.9
20	0.48	16.8
10	3.33	33.6

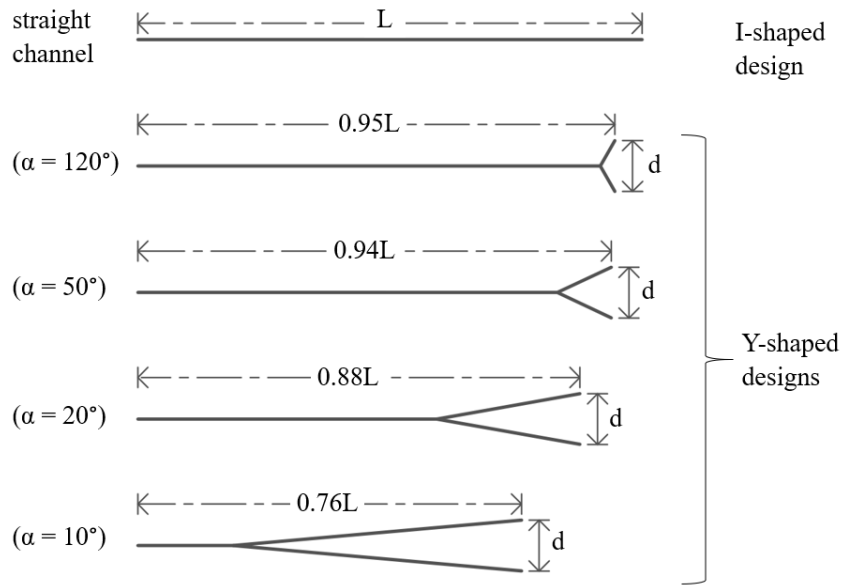


Figure 4: Overview of the different designs.

Remember that the mass flow rate, fluid volume and salt volume are constant. The diameter ratio is always $D_2/D_1 = 2^{-1/2}$ in accord with the constructal law. For example, when the bifurcation angle $\alpha = 20^\circ$, the dendritic configuration corresponds to a length ratio of 0.48. Morphing the geometry from a straight channel to a dendritic one, leads to an overall porous material thickness – from one side to the opposite side of the corresponding porous reactor – of 0.88 L (Fig. 4).

We show in Fig. 5 the reaction advancement as a function of time, obtained in the different configurations of Fig. 4. Time is plotted on the abscissa in a non-dimensional way. The non-dimensional values are related to the moment when the reaction advancement is 1 for the slowest case. The I-shaped configuration is the one needing more time to reach full salt hydration. At the start of the process, the reaction advancements are identical, whatever the channels shape; this is true until the non-dimensional time reaches a value of 0.02. This result is expected as the entrance dimension of each configuration is constant. Then, in time, the salt hydration is faster in

the case of the Y-shaped architectures which in the case $\alpha = 20^\circ$ reaches full hydration for a non-dimensional time of 0.79. In this configuration, the change in geometry comes with an increase of the heat transfer surface of 17% as shown in Table 2, facilitating the diffusion of water molecules through the salt layer and therefore the chemical reaction. The results are confirmed in Fig. 6 where the heat released is plotted as a function of the reaction advancement. The non-dimensional values are based on the heat released in the I-shaped configuration. Even though the salt volume is the same, the change in design allows a maximum increase in heat released of 20% when the bifurcation angle $\alpha = 10^\circ$. Note that the improvement in performance lasts all along the salt hydration process, as the curve corresponding to the Y-shaped design is always 20% above the straight channel configuration in Fig. 6.

Decreasing the bifurcation angle allows to increase the interface between fluid and salt, which in turns leads to a much faster reaction advancement. According to Fig. 5, if the Y-shaped structure has an angle of bifurcation greater than 50° , then the salt hydration advancement is mainly identical to a I-shaped design. The same happens in terms of heat released by the chemical reaction. A small angle between the two daughter channels guaranties a higher heat transfer rate during the entire hydration process (see Fig. 6) as the relative impact of the daughter ducts increases.

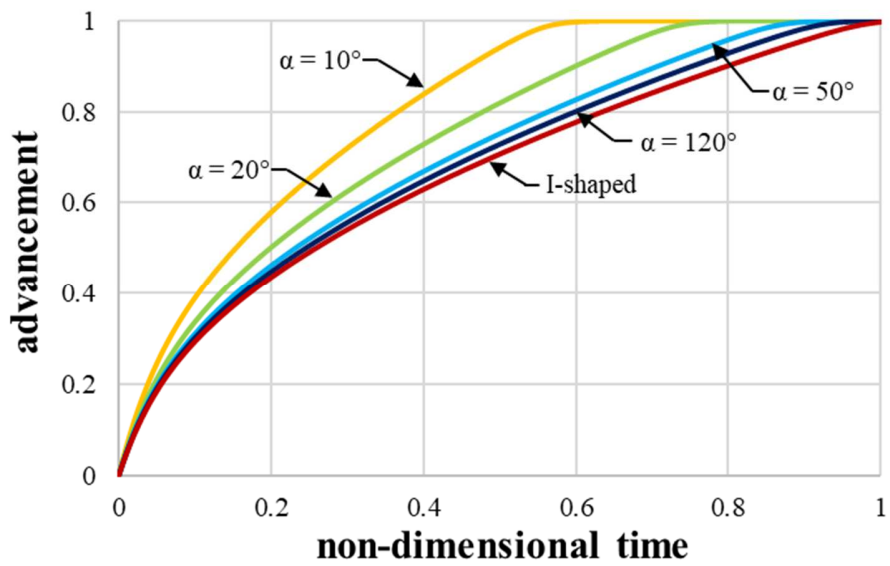


Figure 5: The reaction advancement as a function of the non-dimensional time. Y-shaped configurations with different angles of bifurcation ($\alpha = 10^\circ$, 20° , 50° and 120°) are compared to I-shaped design.

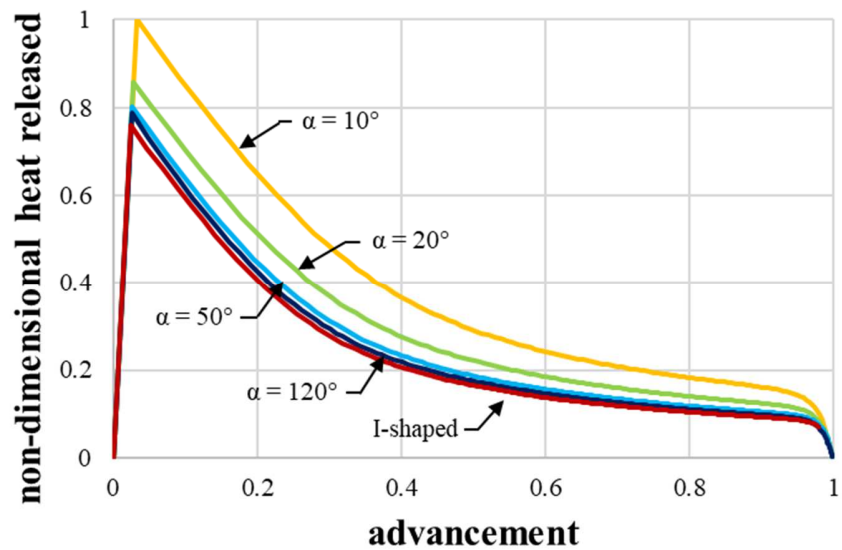


Figure 6: The non-dimensional heat released by the salt chemical reaction as a function of the advancement; Y-shaped configurations with different angles of bifurcation ($\alpha = 10^\circ$, 20° , 50° and 120°) are compared to a I-shaped design.

To get more insight, the full hydration-dehydration process was modeled. The energy performance of the configurations is assessed by dividing the heat transfer rate due to the chemical reaction by the power necessary to blow the fluid through the channels. This ratio is termed β . Next the ratio $\beta_Y / |\beta_{I_{\max}}|$ was calculated. The non-dimensional time is based on the time necessary to complete a full hydration-dehydration cycle which corresponds to the straight channel case.

The evolution of the energy performance indicator β is presented in Fig. 7 for I-shaped and Y-shaped ($\alpha = 20^\circ$) configurations in the case of the full process. The results show that the full cycle for the Y-shaped configuration takes 20% less time than the I-shaped configuration. This feature is favorable for short term storage applications, composed by several hydration-dehydration cycles in a short period. In addition, the absolute value of the β indicator in the Y-shaped configuration is 10% higher than for the I-shaped configuration. Note that the difference in the hydration and dehydration durations is due to the inlet conditions used here (summarized in Table 1). They are taken close to standard reactor operation conditions [31].

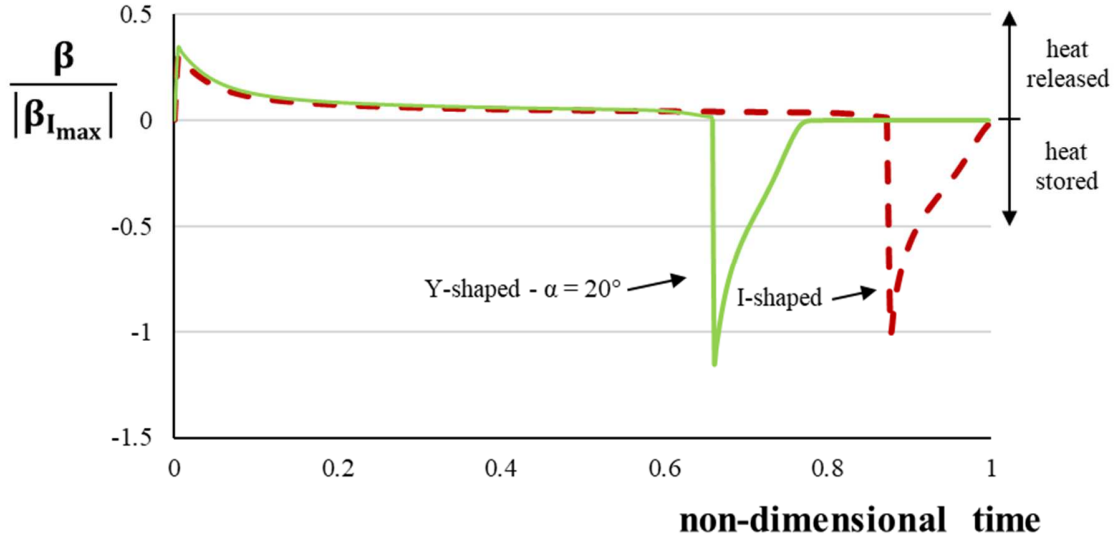


Figure 7: Evolution of the energy performance during a hydration-dehydration cycle for a I-shaped and a Y-shaped configuration. In the latter, the bifurcation angle is $\alpha = 20^\circ$.

Next, the heat exchange surface between fluid and salt was fixed to the one of the I-shaped configuration. The width of the Y-shaped entrance channels varied from $0.94 D$ to $1.09 D$, while $D_2/D_1 = 2^{-1/2}$, the constructal ratio, and d is constant (Table 3). The change in configuration has a null impact on the reaction advancement and the released heat (hydration case) as the heat exchange surface is constant. Impact appears on the fluid mechanics side as the pressure losses vary with D_i^{-4} .

Table 3: Y-shaped configurations with different entrance dimensions D_1 for fixed salt-fluid exchange surface and fixed ratio D_2/D_1 . The bifurcation angle α and length ratio $L_Y/L_{I\text{-shaped}}$ ($L_Y = L_1 + L_2 \cos \frac{\alpha}{2}$) are determined from the previous constraints.

$S/S_{I\text{-shaped}}$	D_2/D_1	D_1/D	α	$L_Y/L_{I\text{-shaped}}$
1	$2^{-1/2}$	0.94	13.2°	0.62

	1	20°	0.75
	1.09	55°	0.90

Table 4: Y-shaped configurations with different ratios D_2/D_1 for fixed salt-fluid exchange surface and fixed entrance dimension. The variation in D_2/D_1 allows to calculate the corresponding bifurcation angle α and length ratio $L_Y/L_{I\text{-shaped}}$ ($L_Y = L_1 + L_2 \cos \frac{\alpha}{2}$).

$S/S_{I\text{-shaped}}$	D_1/D	D_2/D_1	α	$L_Y/L_{I\text{-shaped}}$
1	1	0.83	11.3	0.56
		0.77	15.7	0.68
		$2^{-1/2}$	20.0	0.75
		0.67	22.8	0.78
		0.50	34.5	0.85
		0.40	41.7	0.87
		0.33	46.6	0.88

Table 4 shows the configurations for which the entrance width remains identical to the I-shaped case while again the heat exchange surface is kept constant. Here D_2/D_1 varies and so does α as the spacing d between the two outlets does not change.

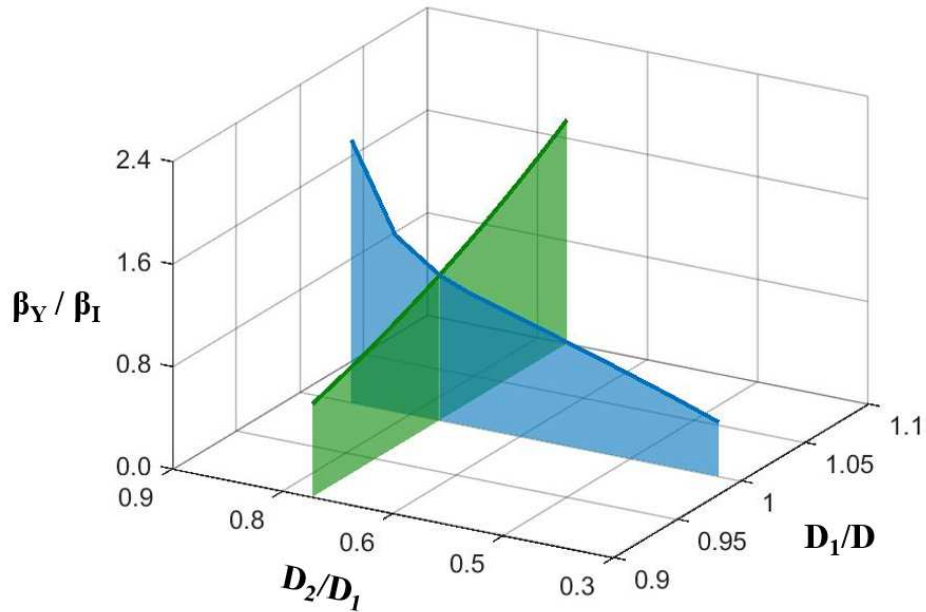


Figure 8: Evolution of the energy performance indicator as a function of the ratio D_2/D_1 for fixed entrance dimension D_1 (blue plane) and as a function of the entrance dimension D_1 for fixed diameter ratio D_2/D_1 (green plane), when the reactor overall thickness is free to vary.

Figure 8 is a summary of the results obtained with Tables 3 and 4. The values presented correspond to a non-dimensional time of 0.005. The design performances can be improved in two ways under the imposed constraints (salt and fluid volume, fluid-salt heat exchange surface): either by increasing the inlet thickness of the Y-shaped networks, or by increasing the daughter-mother channels D_2/D_1 ratio. Either solution is a path to less flow resistances as the fixed heat transfer performance is maintained constant with the heat exchange surface.

More constraining is the problem where the overall material dimensions are fixed. In such case, while the fluid and salt volumes remain unchanged, opportunities to improve both the heat transfer and fluid mechanics aspects exist. This is typically a case when the constructal law provides the directions on how the configurations should evolve. In Table 5, the bifurcation angle

is constant because the exchange surface between fluid and salt and the spacing d between outlets are fixed when the ratio D_2/D_1 changes. The constructal ratio $D_2/D_1 = 2^{-1/2}$ leads to minimum pumping power, while the heat released is insensitive to the morphing of the channels. Therefore the corresponding energy performance indicator is also the highest in this case.

The search for continuous improvement requires to change the bifurcation angle which, based on the constraints, means that α can vary between 8° and 80° . The change in bifurcation angle allows to vary the heat transfer exchange surface as shown in Table 6.

Table 5: Y-shaped configurations with different ratios D_2/D_1 for fixed salt-fluid exchange surface and fixed reactor overall thickness. The bifurcation angle α and the entrance dimensions D_1 are determined from the previous constraints.

$S/S_{I\text{-shaped}}$	α	D_2/D_1	D_1/D
1	20	1.5	1.03
		1.0	1
		$2^{-1/2}$	0.86
		0.5	0.57

Table 6: Y-shaped configurations with different bifurcation angle α for fixed reactor overall thickness and fixed ratio D_2/D_1 . The entrance dimensions D_1 and salt-fluid exchange surfaces are determined from the previous constraints.

D_2/D_1	α	D_1/D	$S/S_{I-shaped}$
$2^{-1/2}$	8	0.63	1.36
	10	0.69	1.24
	20	0.86	1
	40	0.97	0.88
	60	1.01	0.85
	80	1.03	0.83

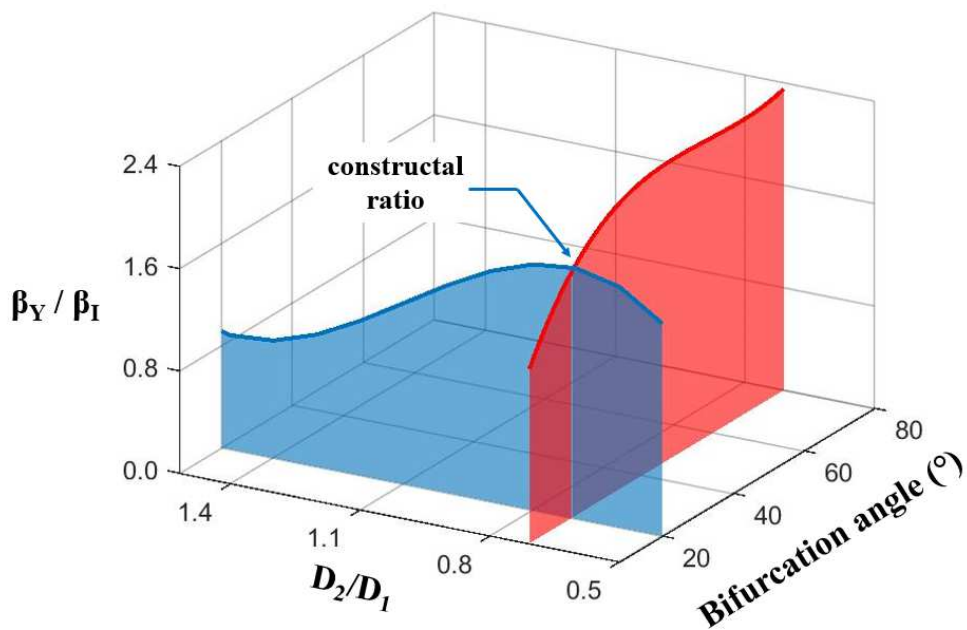


Figure 9: Evolution of the energy performance indicator as a function of the D_2/D_1 ratio for fixed bifurcation angle α (blue plane), and as a function of the bifurcation angle α for fixed ratio D_2/D_1 (red plane), when the overall reactor thickness is fixed.

Figure 9 provides an overview of the results for a non-dimensional time of 0.005. For a fixed angle of bifurcation, the performance map reaches a maximum which corresponds to the daughter-mother channels ratio D_2/D_1 obeying the constructal design methodology. Increasing the energy performance indicator requires to liberate the design configuration and to allow the bifurcation angle to increase which means shorter daughter channels and higher heat transfer exchange surfaces.

Conclusion

The objective of this work was to discover if a drastic change in flow architecture is a way to improve the thermal performance of an elemental configuration for thermochemical energy storage. From the reference case of a straight channel as basic configuration of a pore network part of a reactor, the shape of the pore was moved to a Y-shaped channel made of a main duct and 2 identical daughter channels. The fluid volume was kept constant. The fundamental result of the study is that the Y-shaped configuration leads to a faster reaction advancement and heat released than the I-shaped one.

When the overall thickness of the reactor is allowed to change, the improvements are noteworthy provided the dendritic architecture exhibits an angle of bifurcation smaller than $\alpha = 50^\circ$. In such cases, the morphing Y-shaped configurations permits to increase the heat transfer surface and therefore the thermal performance of the element.

The dramatic change in shape comes with a more compact pore network as the best performances are obtained when the angle of bifurcation decreased to $\alpha = 10^\circ$. This configuration corresponds to a reduction of 25% of the module thickness. A more compact structure leads to increases in the overall thermal and fluid mechanics results.

For a given set of constraints, we can predict how the shape of the pores should evolve in order to benefit the most of a given amount of salt. When maintaining the reactor thickness constant, the main findings are that:

- changing the diameter ratio to the one predicted by the constructal law is the only way to improve the energy performance indicator when the heat transfer exchange surface is fixed.
- the road to more improvements is to be found in allowing the bifurcation angle to increase which leads to more heat exchanges while maintaining the pressure as low as possible.

Finally, this work contributed to highlight the interdisciplinary and versatile nature of the constructal law approach to engineering problems.

Acknowledgements

Alexandre Malley-Ernewein is funded by the French ANR research project DECARTH, ANR-16-CE22-0006-03.

References

- [1] A. Bejan, Constructal tree network for fluid flow between a finite-size volume and one source or sink, *Rev. Générale Therm.* 36 (1997) 592–604.
- [2] A. Bejan, S. Lorente, Constructal tree-shaped flow structures, *Appl. Therm. Eng.* 27 (2007) 755–761.
- [3] W. Wechsatoł, S. Lorente, A. Bejan, Tree-shaped insulated designs for the uniform distribution of hot water over an area, *Int. J. Heat Mass Transf.* 44 (2001) 3111–3123.
- [4] V.D. Zimparov, A.K. da Silva, A. Bejan, Constructal tree-shaped parallel flow heat exchangers, *Int. J. Heat Mass Transf.* 49 (2006) 4558–4566.
- [5] G.A. Ledezma, A. Bejan, M.R. Errera, Constructal tree networks for heat transfer, *J. Appl. Phys.* 82 (1997) 89–100.
- [6] W. Wechsatoł, S. Lorente, A. Bejan, Optimal tree-shaped networks for fluid flow in a disc-shaped body, *Int. J. Heat Mass Transf.* 45 (2002) 4911–4924.
- [7] A. Bejan, S. Lorente, *Design with Constructal Theory*, John Wiley & Sons, Hoboken, 2008.
- [8] T. Watzek, S. Lorente, From pore network prediction based on the Constructal law to macroscopic properties of porous media, *J. Phys. Appl. Phys.* 48 (2015).
- [9] A. Bejan, L.A.O. Rocha, S. Lorente, Thermodynamic optimization of geometry: T- and Y-shaped constructs of fluid streams, *Int. J. Therm. Sci.* 39 (2000) 949–960..
- [10] W. Wechsatoł, S. Lorente, A. Bejan, Dendritic heat convection on a disc, *Int. J. Heat Mass Transf.* 46 (2003) 4381–4391.
- [11] A.F. Miguel, Constructal branching design for fluid flow and heat transfer, *Int. J. Heat Mass Transf.* 122 (2018) 204–211..
- [12] E. Cetkin, A.F. Miguel, Constructal branched micromixers with enhanced mixing efficiency: Slender design, sphere mixing chamber and obstacles, *Int. J. Heat Mass Transf.* 131 (2019) 633–644..
- [13] A. Bejan, Thermodynamics of heating, *Proc. R. Soc. Math. Phys. Eng. Sci.* 475 (2019) 20180820.
- [14] S. Lorente, A. Bejan, Current trends in constructal law and evolutionary design, *Heat Transfer Asian Res.* 48 (2019) 3574–3589.
- [15] S. Lorente, A. Bejan, J.L. Niu, Constructal design of latent thermal energy storage with vertical spiral heaters, *Int. J. Heat Mass Transf.* 81 (2015) 283–288.
- [16] S. Ziaei, S. Lorente, A. Bejan, Constructal design for convection melting of a phase change body, *Int. J. Heat Mass Transf.* 99 (2016) 762–769.
- [17] V. Joshi, M.K. Rathod, Constructal enhancement of thermal transport in metal foam-PCM composite-assisted latent heat thermal energy storage system, *Numer. Heat Transf. Part Appl.* 75 (2019) 413–433.

- [18] J.H. Nazzi Ehms, R. De Césaró Oliveski, L.A. Oliveira Rocha, C. Biserni, Theoretical and numerical analysis on phase change materials (PCM): A case study of the solidification process of erythritol in spheres, *Int. J. Heat Mass Transf.* 119 (2018) 523–532.
- [19] A. Solé, Q. Falcoz, L.F. Cabeza, P. Neveu, Geometry optimization of a heat storage system for concentrated solar power plants (CSP), *Renew. Energy.* 123 (2018) 227–235.
- [20] G. Xie, Y. Song, M. Asadi, G. Lorenzini, Optimization of Pin-Fins for a Heat Exchanger by Entropy Generation Minimization and Constructal Law, *J. Heat Transf.* 137 (2015).
- [21] B. Guene Lougou, Y. Shuai, R. Pan, G. Chaffa, H. Tan, Heat transfer and fluid flow analysis of porous medium solar thermochemical reactor with quartz glass cover, *Int. J. Heat Mass Transf.* 127 (2018) 61–74.
- [22] C. Lehmann, O. Kolditz, T. Nagel, Modelling sorption equilibria and kinetics in numerical simulations of dynamic sorption experiments in packed beds of salt/zeolite composites for thermochemical energy storage, *Int. J. Heat Mass Transf.* 128 (2019) 1102–1113.
- [23] A. Malley-Ernewein, S. Lorente, Constructal design of thermochemical energy storage, *Int. J. Heat Mass Transf.* 130 (2019) 1299–1306.
- [24] A. Malley-Ernewein, S. Lorente, Analysis of thermochemical energy storage in an elemental configuration, *Sci. Rep.* 9 (2019) 1–9.
- [25] S. Lorente, A. Bejan, Heterogeneous porous media as multiscale structures for maximum flow access, *J. Appl. Phys.* 100 (2006) 114909.
- [26] A. Bejan, *Convection heat transfer*, 4th ed., Wiley, Hoboken, 2013.
- [27] S. Lorente, A. Bejan, Svelteness, freedom to morph, and constructal multi-scale flow structures, *Int. J. Therm. Sci.* 44 (2005) 1123–1130.
- [28] B. Michel, N. Mazet, P. Neveu, Experimental investigation of an open thermochemical process operating with a hydrate salt for thermal storage of solar energy: Local reactive bed evolution, *Appl. Energy.* 180 (2016) 234–244.
- [29] H.L. Langhaar, Steady flow in the transition length of a straight tube, *J. Appl. Mech.* 9 (1942).
- [30] COMSOL Multiphysics, n.d.
- [31] B. Michel, N. Mazet, P. Neveu, Experimental investigation of an innovative thermochemical process operating with a hydrate salt and moist air for thermal storage of solar energy: Global performance, *Appl. Energy.* 129 (2014) 177–186.